PERGAMON

Journal of Quantitative Spectroscopy & Radiative Transfer 82 (2003) 413–428

Journal of Quantitative Spectroscopy & Radiative Transfer

www.elsevier.com/locate/jqsrt

The infrared absorption cross-section and refractive-index data in HITRAN

S.T. Massie[a,*], A. Goldman[b]

[a] *National Center for Atmospheric Research, 1850 Table Mesa Dr. P.O. Box 3000, Boulder, CO 80307, USA*
[b] *Department of Physics, University of Denver, Denver, CO 80208, USA*

Received 16 January 2003; received in revised form 14 March 2003; accepted 17 March 2003

Abstract

The cross-sections and indices of refraction on the HIgh-resolution TRANsmission (HITRAN) database are summarized. HITRAN contains a tabulation of cross-sections of atmospheric chemical reservoir and source species, chlorofluorocarbons, hydrochlorofluorocarbons, and hydrofluorocarbons, and indices of refraction of liquid and solid compounds. The temperature and pressure dependences of the cross-sections and the temperature dependence of the indices of refraction are illustrated. Data uncertainties and applications are discussed, and some future needs of the remote-sensing community are identified.

Keywords: Cross-sections; Refractive-indices; Infrared; HITRAN; CFC; HCFC; HFC; Aerosol

1. Introduction

The infrared opacity of the atmosphere is due to both gaseous molecules, and liquid and solid aerosol particles. The HIgh resolution TRANsmission (HITRAN) database [1] contains a tabulation of cross-sections of molecules for which line-by-line spectroscopic parameters are not yet available. Indices of refraction of liquid and solid compounds, that are needed to calculate aerosol extinction spectra, are also tabulated. As illustrated in figures in this paper, the cross-sections and indices of refraction contribute to atmospheric opacity throughout the infrared.

Previous editions of the HITRAN database [2] contained a tabulation of cross-section and indices of refraction for many species and compounds. HITRAN now has a substantial tabulation of the cross-sections of hydrochlorofluorocarbon (HCFC) and hydrofluorocarbon (HFC) species, and indices of refraction of important aerosols at stratospheric temperatures. The development and content of the

* Corresponding author. Tel.: 1-303-497-1404; fax: 1-303-497-1492.
E-mail address: massie@ucar.edu (S.T. Massie).

0022-4073/03/$ - see front matter
doi:10.1016/S0022-4073(03)00167-5

HITRAN database during the last two decades reflects advances in atmospheric science, specifically research focusing upon remote sensing of trace species, the impact of chlorofluorocarbons (CFCs) upon the ozone layer, the industrial utilization of CFC replacements (i.e. the HCFCs and HFCs), and the effects of polar stratospheric clouds (PSCs) upon polar chemistry.

The paper has been organized as follows. Section 2 is a review of the infrared cross-sections that are in the HITRAN database. Examples of the dependence of the cross-sections on temperature and pressure, and a discussion of applications, are presented. Section 3 is a review of the HITRAN refractive indices and their dependence upon temperature, along with the applications of these data. A brief discussion of applications is also presented. Section 4 is a discussion of the laboratory measurements that are needed to improve the cross-sections and refractive indices in HITRAN.

2. Cross-sections

2.1. Background information

Atmospheric chemical reservoir species such as N_2O_5, $ClONO_2$, and HNO_4 sequester reactive nitrogen and chlorine via the reactions

$$NO_2 + NO_3 + M \rightarrow N_2O_5 + M, \tag{1}$$

$$ClO + NO_2 + M \rightarrow ClONO_2 + M, \tag{2}$$

$$NO_2 + HO_2 + M \rightarrow HNO_4 + M, \tag{3}$$

where M is a third body (N_2 or O_2). These reactions decrease the atmospheric concentrations of NO_2 and ClO, which otherwise would participate in catalytic reactions that destroy ozone in the stratosphere.

$ClONO_2$, however, reacts with HCl on polar stratospheric cloud particles. This heterogeneous reaction releases Cl_2, which is readily photolyzed into active chlorine (Cl) in the presence of sunlight

$$ClONO_2(g) + HCl(s) \rightarrow Cl_2 + HNO_3. \tag{4}$$

These reactions take place on solid particles such as nitric acid trihydrate (NAT). Similar reactions also occur on liquid $H_2O/H_2SO_4/HNO_3$ droplets. Indices of refraction of NAT and other PSC candidate compounds are discussed in Section 3 of this paper.

The introduction of CFCs into the troposphere, especially CFC-11 and CFC-12, has resulted in the enhancement of the total active chlorine content of the atmosphere via photolytic reactions such as

$$CCl_2F_2 + h\nu \rightarrow CF_2Cl + Cl \tag{5}$$

followed by further decomposition of CF_2Cl. The CFC gases also enhance the greenhouse effect by absorbing in the infrared window between 8 and 12 μm. International treaties such as the Montreal Protocol, and subsequent London and Copenhagen Amendments, have established the phaseout of CFCs and HCFCs. HFCs will eventually be used for refrigeration purposes. Hydrohalocarbons contain at least one hydrogen atom, react with the hydroxyl radical (OH) in the troposphere, and thereby

deposit less chlorine into the stratosphere than the CFC compounds. Hydrohalocarbons do contribute to greenhouse warming, and their global warming potentials [3] have been estimated using the data sets that are included in the HITRAN database [4,5]. Monitoring of CFCs, HCFCs, and HFCs [6,7] is an important observational task since the decrease in tropospheric chlorine from a peak of 3.7 ppbv in 1994 to levels near 2 ppbv, the threshold at which the onset of the Antarctic ozone hole was observed, will likely occur by 2050. See [8] for a general discussion of halogen chemistry.

Heavy molecules have large moments of inertia, therefore the spacing between rovibrational lines of heavy molecules is very small, and the band structure is a blending of numerous individual spectral features. The number of individual lines for species such as CFC-12 is on the order of 100 times that of H_2O or CO_2, for instance. The presence of various Cl isotopic lines and hot bands further complicates laboratory analyses of CFC spectra. These complications have delayed the development of heavy molecule line listings. For gases whose line parameters are not yet available, HITRAN contains cross-sections derived from laboratory spectra at atmospheric pressures and temperatures. For example, HITRAN includes supplemental line listings of SF_6 and $ClONO_2$.

2.2. HITRAN files and format

Cross-sections are presented in ASCII format. In each file, each band has a separate header stating the molecule name, the range of wavenumber for the band, number of data points, and the temperature and pressure of the laboratory measurements. Cross-sections are in cm^2/molecule units. Negative cross-sections in the original laboratory data sets have been set to zero, due to instrumental noise that was significant in measurements performed at low optical depths.

We list in Table 1 the molecules, and the pressure and temperature conditions of the laboratory data. Temperatures range from 180 to 297 K. Pressures range from 760 Torr to air-broadening near zero pressure. It should be noted that the data obtained at high spectral resolution (e.g. 0.002 cm^{-1}) are usually not significantly different from the data obtained at lower resolution (of the order of 0.02 cm^{-1}). Cross-sections were measured in different laboratories at different temperatures and pressures, and thus, multiple tabulations are currently included in the database.

2.3. Temperature and pressure dependence

We present in Figs. 1–3 representative cross-sections of CFC-12 [5], HFC-134a [23], and $ClONO_2$ [11] to illustrate the temperature and pressure dependences of the cross-sections of heavy molecules. In Figs. 1 and 2 we demonstrate that individual bands of heavy molecules usually span approximately 60 cm^{-1}. Q-branches are the most prominent spectral features in many remote sensing observations, so quantification of these spectral features is of particular interest. It is apparent in Figs. 1–3 that accurate quantification of the temperature and pressure dependencies of heavy molecule cross-sections is required for accurate remote sensing applications. Cross-sections vary by a factor of 2 for CFC-12 and a factor of 2.5 for HFC-134a in Figs. 1 and 2, respectively, for the range of pressures and temperatures in the troposphere. Arrows are used in Figs. 1 and 2 to identify these variations. Individual temperature and pressure dependencies are illustrated in Fig. 3. The cross-section at 780.2 cm^{-1} in the Q-branch of $ClONO_2$ increases by 72% as the temperature drops from 249 to 189 K at a pressure of 25 hPa, and increases by 23% as air-broadened pressure drops from 45 to 12 hPa at 189 K.

Table 1
Summary of the refractive indices listed in HITRAN

Molecule	Name	T (K)	P (Torr)	Sets	Wavenumber (cm^{-1})	References
SF_6	Sulfur hexafluoride	180–295	20–760	32	925–955	[9]
$ClONO_2$	Chlorine nitrate	213–296	0	2	740–840	[10]
		213–296	0	2	1240–1340	
		213–296	0	2	1680–1790	
$ClONO_2$	Chlorine nitrate	189–297	0–155	23	689–1330	[11]
		213–296	0	2	1680–1790	
CCl_4	Carbon tetrachloride	208–297	8–760	32	750–812	[12]
N_2O_5	Dinitrogen pentoxide	233–293	0	4	555–600	[13]
		233–293	0	4	720–765	
		233–293	0	4	1210–1275	
		233–293	0	4	1680–1765	
N_2O_5	Dinitrogen pentoxide	205–293	0	5	540–1380	[14]
C_2F_6	Hexafluoro-ethane	181–296	25–760	43	1061–1165	[15]
		181–296	25–760	43	1229–1285	
HNO_4	Pernitric acid	268	0.7	1	770–830	[16]
CCl_3F	CFC-11	190–296	8–760	55	810–880	[17]
		190–296	8–760	55	1050–1120	
CCl_2F_2	CFC-12	190–296	7.5–760	52	850–950	[5,17]
		190–296	7.5–760	52	1050–1200	
$CClF_3$	CFC-13	203–293	0	6	765–805	[18,19]
		203–293		6	1065–1140	
		203–293		6	1170–1235	
CF_4	CFC-14	180–296	7.5–761	55	1250–1290	[20]
$C_2Cl_3F_3$	CFC-113	203–293	0	6	780–995	[18]
		203–293	0	6	1005–1232	
$C_2Cl_2F_4$	CFC-114	203–293	0	6	815–860	[18]
		203–293	0	6	870–960	
		203–293	0	6	1030–1067	
		203–293	0	6	1095–1285	
C_2ClF_5	CFC-115	203–293	0	6	955–1015	[18]
		203–293	0	6	1110–1145	
		203–293	0	6	1167–1260	
$CHCl_2F$	HCFC-21	296	1	1	785–840	[16]
$CHClF_2$	HCFC-22	181–297	0–765	29	760–860	[9]
		181–297	0–761	34	1070–1195	[4,9]
		253–287	0	3	1275–1380	[4]
$CHCl_2CF_3$	HCFC-123	253–287	0	3	740–900	[4]
		253–287		1	1079–1450	
$CHClFCF_3$	HCFC-124	287	0	1	675–715	[4]
		287	0	1	790–920	
		287	0	1	1035–1430	
CH_3CCl_2F	HCFC-141b	253–287	0	3	710–790	[4]
		253–287	0	3	895–1210	
		253–287	0	3	1325–1470	
CH_3CClF_2	HCFC-142b	253–287	0	3	650–705	[4]
		253–287	0	3	875–1265	
		253–287	0	3	1360–1475	

Table 1 (*continued*)

Molecule	Name	T (K)	P (Torr)	Sets	Wavenumber (cm^{-1})	References
$CHCl_2CF_2CF_3$	HCFC-225ca	253–287	0	3	695–865	[4]
		253–287	0	3	1010–1420	
$CClF_2CF_2CHClF$	HCFC-225cb	253–287	0	3	715–1375	[4]
CH_2F_2	HFC-32	203–297	0–750	17	995–1236	[21]
		203–297	0–750	17	1385–1475	
CHF_2CF_3	HFC-125	287	0	1	700–745	[4]
		287	0	1	840–890	
		287	0	1	1060–1465	
CHF_2CHF_2	HFC-134	203–297	0–750	9	600–1700	[22]
CFH_2CF_3	HFC-134a	253–287	0	3	815–865	[4]
		253–287	0	3	935–1485	
		190–296	20–760	32	1035–1130	[23]
		190–296	20–760	34	1135–1340	
CF_3CH_3	HFC-143a	203–297	0–750	9	580–630	[22]
		203–297	0–750	9	750–1050	
		203–297	0–750	9	1100–1500	
CH_3CHF_2	HFC-152a	253–287	0	3	840–995	[4]
		253–287	0	3	1050–1205	
		253–287	0	3	1320–1490	

2.4. Comparison of data

The absolute accuracy of the cross-section data is typically 5–10% for the infrared cross-sections listed in Table 1. We present in Fig. 4 the cross-sections of N_2O_5 from Refs. [13,14] to illustrate a typical inter-comparison of the data.

Cantrell [13] measured cross-sections for N_2O_5 between 233 and 296 K. Cross-sections were measured at spectral resolutions between 0.03 and 0.5 cm^{-1}, showing small sensitivity to the resolution. In Fig. 4 we compare these cross-sections with those of Birk and Wagner [14] at temperatures of 293 and 253 K and a resolution of 0.008 cm^{-1}. Room temperature data are in excellent agreement in the top panel of Fig. 4, and the data at 253 K in the bottom panel differ by 7%.

2.5. Utilization of the data

For a path segment increment of length ds (cm) with number density n (molecules cm^{-3}) for a particular species, the optical depth contribution to the path segment is $\sigma(P,T,v)n\,\mathrm{d}s$, where $\sigma(P,T,v)$ is the cross-section (cm^2/molecule) of the species at pressure P, temperature T, and wavenumber v. Interpolation can be used to specify cross-section values for pressure and temperature conditions between those that are tabulated in the HITRAN database.

With the availability of current computer storage capacity, it is possible to create files of cross-sections for a matrix of pressure and temperature conditions, based upon the HITRAN database, and use these files in radiative transfer calculations. It should be noted that the cross-sections of the far wings for some bands become too small and are dominated by the noise level of the laboratory measurement.

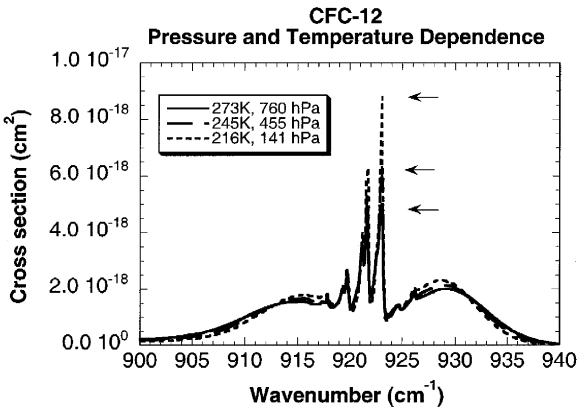

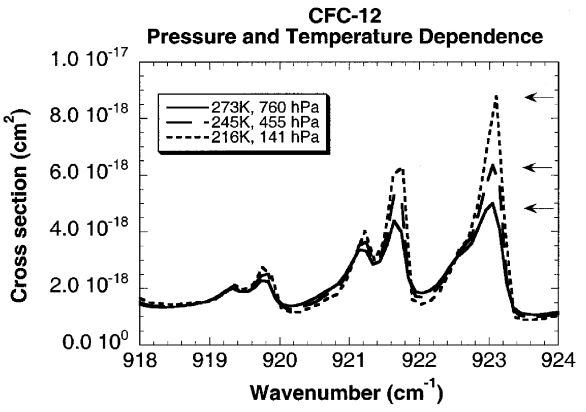

Fig. 1. Cross-sections of CFC-12 vapor [5] at representative tropospheric temperatures and pressures. Arrows mark peak Q-branch cross-section values.

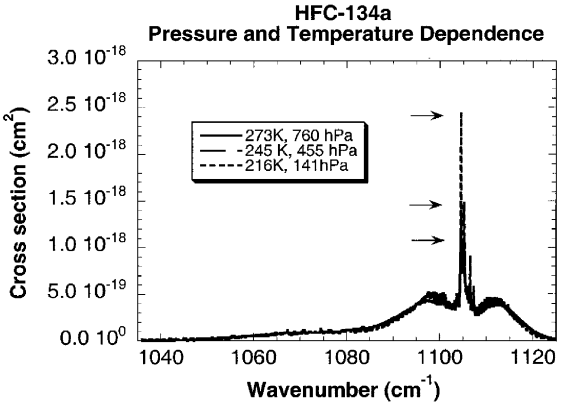

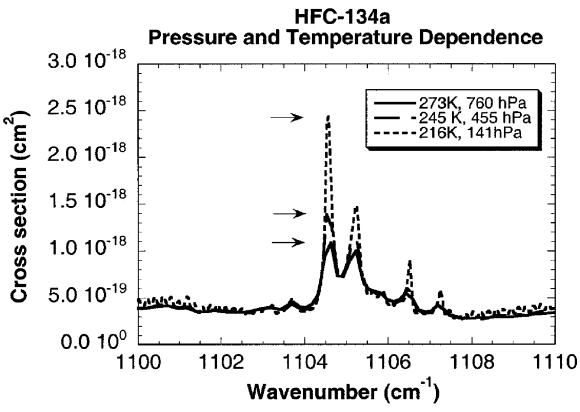

Fig. 2. Cross-sections of HFC-134a vapor [23] at representative tropospheric temperatures and pressures. Arrows mark peak Q-branch cross-section values.

3. Refractive indices

3.1. Background information

Aerosol particles and gas molecules contribute to atmospheric infrared opacity and influence atmospheric chemistry and radiative transfer. Stratospheric sulfuric acid aerosol (i.e. H_2SO_4/H_2O droplets), polar stratospheric cloud (PSC) aerosol, cirrus near the tropopause, and tropospheric cloud droplets, are examples of particle types that are present in the Earth's atmosphere. Heterogeneous chemistry on stratospheric sulfuric acid aerosol alters the partitioning of NO_2, HNO_3, N_2O_5, and NO_x (i.e. NO_2 and NO), and the PSCs are responsible for the creation of the "ozone hole" phenomena [24]. The radiative effects of cloud particles (solid and liquid) in the troposphere are uncertain, and a focus of current research [25].

The opacity of particles is dependent upon composition by way of the refractive index

$$n(\lambda) = n_r - \mathrm{i}n_{im}, \tag{6}$$

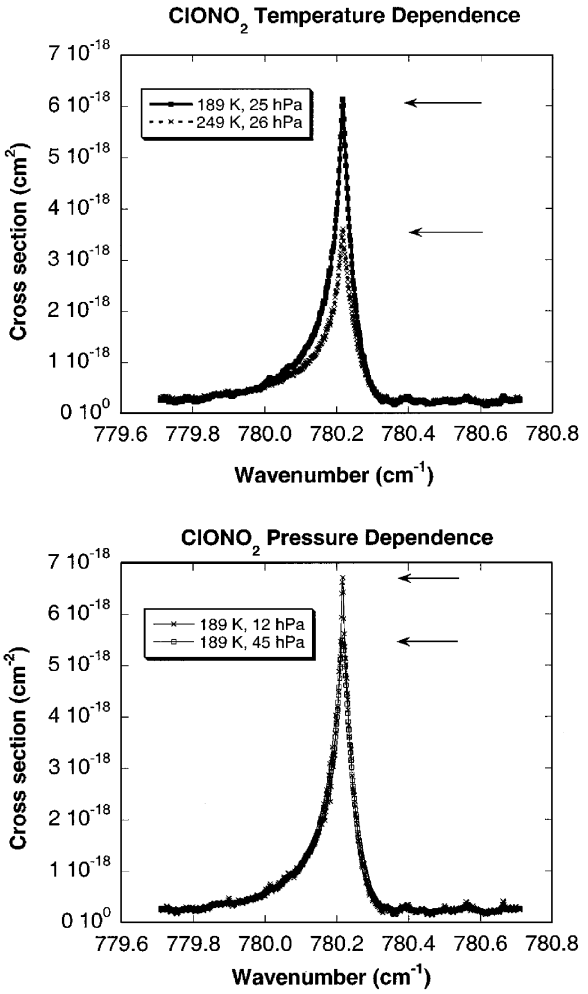

Fig. 3. The temperature and pressure dependences of heavy molecules are illustrated using the $ClONO_2$ vapor Q-branch cross-sections [11] near 780.2 cm^{-1}.

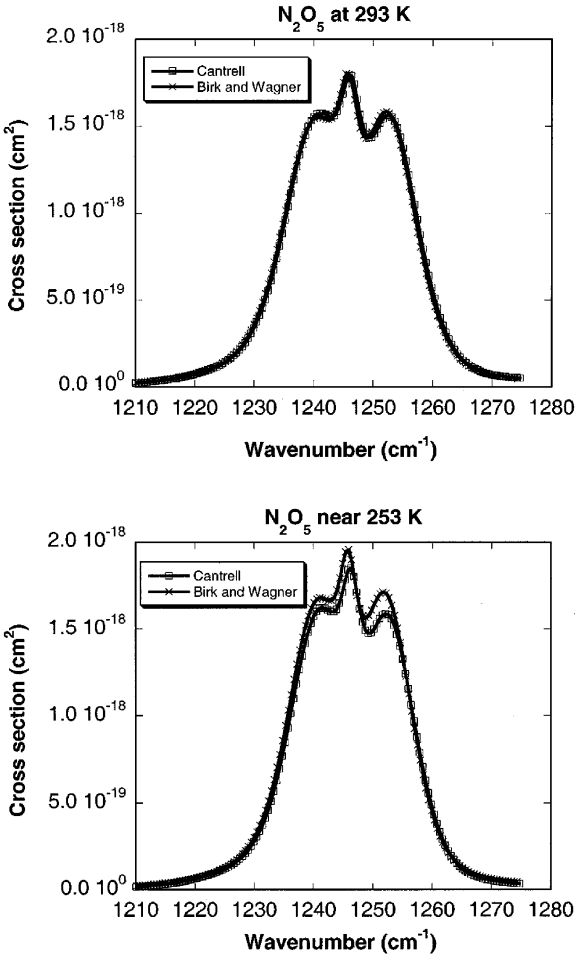

Fig. 4. Intercomparison of N_2O_5 vapor cross-sections [13,14]. In the lower panel the Cantrell [13] and Birk and Wagner [14] cross-sections are at 253 and 254 K, respectively.

where λ is the wavelength of light, n_r is the real refractive index, and n_{im} is the imaginary refractive index. In a medium with complex index $n(\lambda)$, the amplitude of the electric field traveling in the positive z direction has the form

$$E = \exp[-\omega n_{im} z/c]\exp[i\omega(t - n_r z/c)], \tag{7}$$

where c is the speed of light, ω is the circular frequency of the wave, and t is time. Thus, the imaginary part of the complex refractive index produces absorption of light in the medium.

Particle composition and indices of refraction change as ambient conditions of temperature and gas phase mixing ratios vary. For example, the variation of the weight percent content of H_2SO_4

for sulfuric acid aerosol for temperatures between 190 and 260 K, as a function of the ambient H_2O partial pressure, is presented in Fig. 3 of [26]. Accordingly, the refractive index of sulfuric acid aerosol is tabulated in HITRAN as a function of temperature and the H_2SO_4/H_2O weight percent.

As temperatures decrease, e.g. below 195 K for altitudes near 20 km, vapor of HNO_3 is incorporated into the liquid sulfuric acid droplet, which becomes a ternary droplet. Theoretical specifications of the ternary ($H_2SO_4/HNO_3/H_2O$) system [27] can be used to calculate the H_2SO_4 and HNO_3 contents of the liquid droplet in terms of gas phase H_2O, HNO_3, and H_2SO_4 mixing ratios, pressure, and temperature. As discussed below in Section 3.3, accurate indices of refraction of the ternary droplet for a range of stratospheric temperature are yet to be measured.

Remote-sensing observations of aerosol are used frequently to determine the wavelength dependent extinction coefficient, k_{ext} (km^{-1}), of the aerosol. For a path increment of length ds (km), the corresponding increment in optical depth along the path segment is $k_{\text{ext}}\,\text{d}s$.

The extinction coefficient of a spherical particle is

$$k_{\text{ext}} = 10^{-3} \int Q_{\text{ext}}[x, n(\lambda)]\pi r^2\,\text{d}N/\text{d}r\,\text{d}r, \tag{8}$$

where Q_{ext} is the Mie efficiency factor (dimensionless), r is the particle radius (μm), dN/dr (particles $\text{cm}^{-3}\ \mu\text{m}^{-1}$) is the particle size distribution, and the particle size parameter x is equal to $2\pi r/\lambda$ (dimensionless). Extinction refers to the removal (both scattering and absorption) of photons from a beam of light. The efficiency factors for scattering (Q_{sca}) and absorption (Q_{abs}) are related to Q_{ext} by

$$Q_{\text{ext}} = Q_{\text{sca}} + Q_{\text{abs}} \tag{9}$$

and

$$k_{\text{ext}} = k_{\text{sca}} + k_{\text{abs}}. \tag{10}$$

The factor of 10^{-3} in Eq. (8) is used to convert k_{ext} from m^{-1} to km^{-1}, a unit commonly used in atmospheric aerosol research. Mie theory is discussed in several references [28,29].

For solid particles that are nonspherical, e.g. ice crystals and polar stratospheric hydrates, scattering and absorption coefficients are calculated using T-matrix [30,31] and other methods [32]. Particle size and shape both determine the angular distribution by which a particle scatters light, e.g. particle shape can have an important effect on the ratio of forward to backward scattered intensities.

Finally, the radiation field in an atmosphere that includes particles is calculated using specialized computer codes. Particles which mostly scatter, or mostly absorb, have different effects upon the radiation field. Refs. [33,34] discuss the calculation of atmospheric radiation fields.

3.2. HITRAN files and format

There is a separate ASCII file for each refractive-index data set. The header of each file describes the data, cites a journal reference, specifies an email address of a person from the laboratory that measured the indices, and provides the format specification of the tabulation. The data portion of the file tabulates the real and imaginary indices as a function of wavelength, temperature, and appropriate weight percent (e.g., H_2SO_4 weight percent for H_2SO_4/H_2O indices).

Table 2
Summary of the refractive indices listed in HITRAN

Compound	Measurement specifics	References
Water	27°C, 10–5000 cm^{-1}	[35]
Water	0.67–2.5 μm	[36]
Ice	−7°C, 0.04–167 μm −1°C to −60°C, 167 μm–8 m	[37]
Ice	0.67–2.5 μm	[36]
Ice	130–210 K, 800–4004 cm^{-1}	[38]
Ice	166–196 K, 4000–7000 cm^{-1}	[39]
Water, ice, sodium chloride, sea salt, water soluble aerosol, ammonium sulfate, carbonaceous aerosol, volcanic dust, sulfuric acid, meteoric dust, quartz, hematite, sand	Room temperature, 0.2–40 μm	[40–43]
Sulfuric acid (H_2SO_4/H_2O)	Room temperature, 25–96% H_2SO_4	[44]
Sulfuric acid (H_2SO_4/H_2O)	Room temperature, 75 and 90% H_2SO_4	[45]
Sulfuric acid (H_2SO_4/H_2O)	215 K, 499–6996 cm^{-1}	[46]
Sulfuric acid (H_2SO_4/H_2O)	200–300 K, 825–4700 cm^{-1}	[47]
Sulfuric acid (H_2SO_4/H_2O)	213–293 K, 432–5028 cm^{-1}	[48]
Nitric acid (H_2SO_4/HNO_3)	Room temperature, 250–2987 cm^{-1}	[49]
Nitric acid (H_2SO_4/HNO_3)	220 K, 754–4700 cm^{-1}	[50]
Nitric acid (H_2SO_4/HNO_3)	213–293 K, 432–5028 cm^{-1}	[48]
Amorphous nitric acid (NAM, NAD, NAT)	153 K, 482–7000 cm^{-1}	[51]
NAM	179 K, 482–6002 cm^{-1}	[51]
NAD	184 K, 482–6981 cm^{-1}	[51]
NAD	160–190 K, 700–4700 cm^{-1}	[47]
αNAT	181 K, 482–6989 cm^{-1}	[51]
βNAT	196 K, 482–6364 cm^{-1}	
NAT	160 K, 711–4004 cm^{-1}	[52]
Organic based nonvolatile aerosols	525–5000 cm^{-1}	[53]

Table 2 lists the indices in the HITRAN database. There are refractive-index data on 21 compounds in 23 separate data files. There are appreciable uncertainties of the indices for some of the compounds, and thus, multiple tabulations are included in HITRAN.

3.3. Temperature dependence and accuracies of the data

To illustrate the temperature dependence and the accuracies of the data, we intercompare ice, NAT, H_2SO_4/H_2O and HNO_3/H_2O indices from several laboratories. These examples highlight the range of accuracy of current refractive-index measurements.

We present in Fig. 5 water ice indices from Refs. [37,39,51]. Warren [37] tabulated the real and imaginary indices of ice at wavelengths between 4.4×10^{-2} and 8.6×10^{6} μm (2.3×10^{5} to 1.2×10^{-3} cm^{-1}). As discussed by Warren, tabulation of two sets of complex indices is not necessary since the ice crystal is only slightly birefringent (i.e. the indices of refraction differ for directions along and orthogonal to the crystal optic axis). Toon et al. [51] determined indices by applying

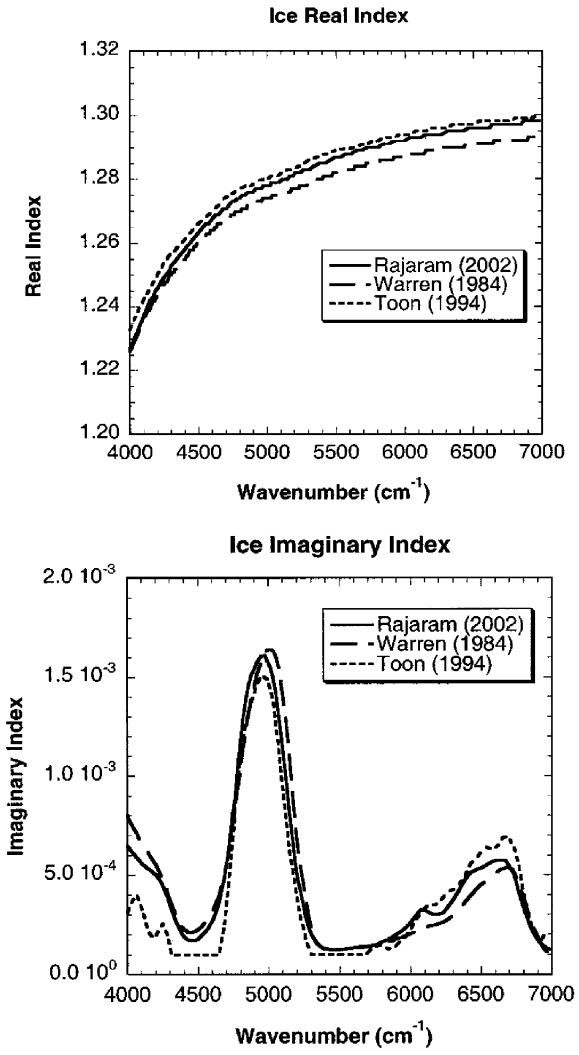

Fig. 5. Intercomparison of real and imaginary refractive-indices of water ice [37,39,51].

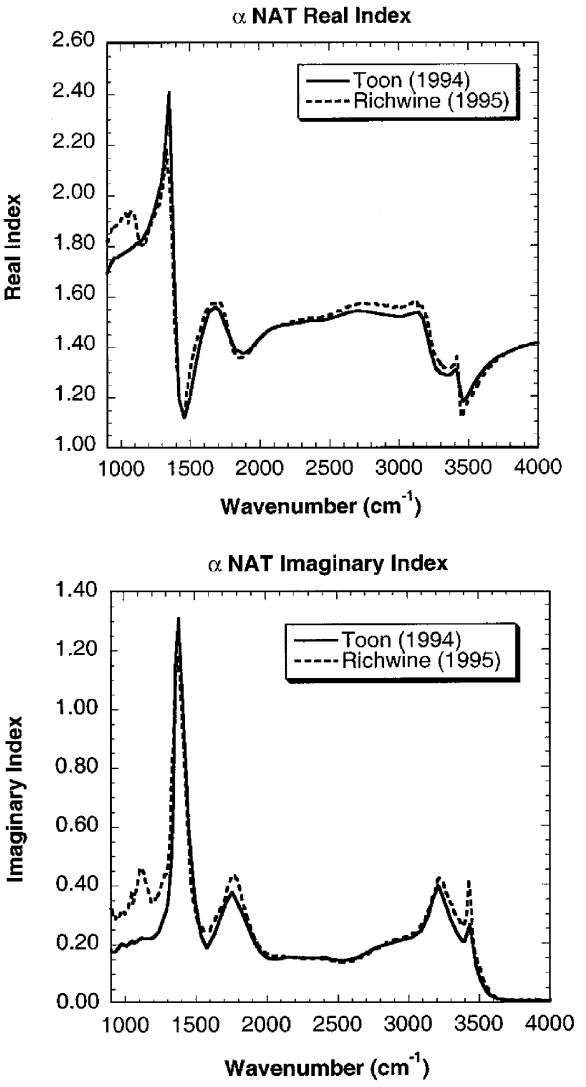

Fig. 6. Intercomparison of the real and imaginary refractive-indices of αNAT [51,52].

an iterative Kramers–Kronig technique that accounted for the radiative transfer through a substrate that has thin films on both sides of the substrate. Recent measurements [39] at 166, 176, 186, and 196 K also applied this methodology. Rajaram et al. [39] note that there is no noticeable temperature dependence of the ice indices, and this is consistent with the 0.1% change predicted by the Lorentz–Lorenz equation. Real indices agree to within 0.25% in Fig. 5. Imaginary indices agree to 10% for the peaks in Fig. 5, while there are appreciable differences for low values of absorption.

A comparison of NAT (nitric acid trihydrate) [51,52] refractive indices is displayed in Fig. 6. NAT is one of several possible solid PSC composition types, and forms at temperatures above the ice

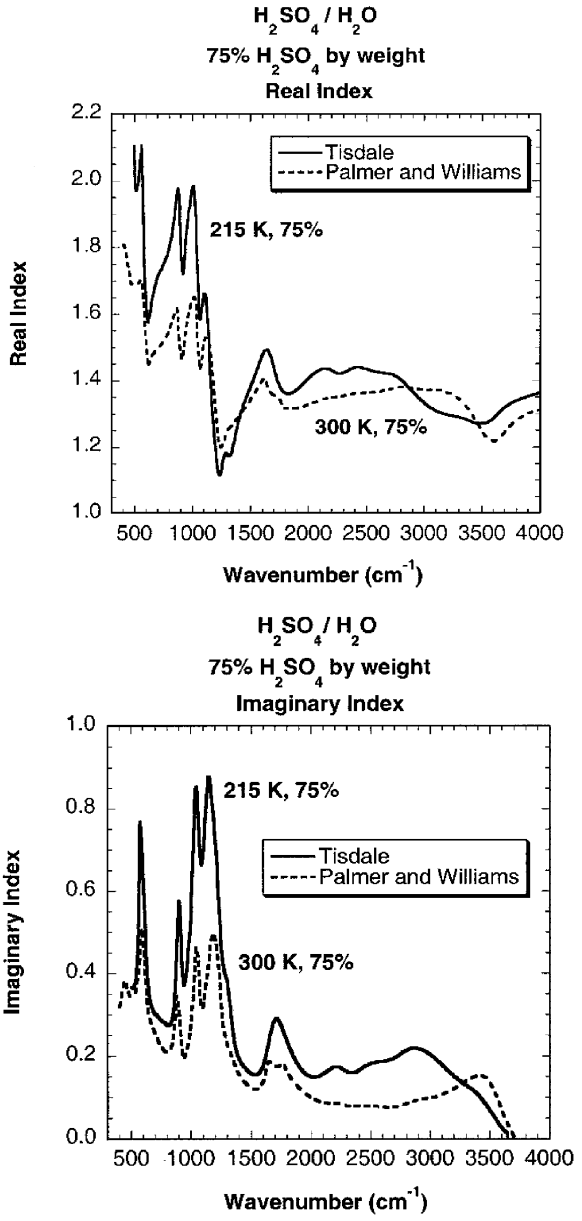

Fig. 7. The temperature dependence of the real and imaginary refractive indices of H_2SO_4/H_2O indices is illustrated by comparing indices at room and stratospheric temperatures [44,46].

frost point. Nitric acid monohydrate (NAM), nitric acid dihydrate (NAD), and nitric acid trihydrate (NAT) have stoichiometric H_2O/HNO_3 ratios of 1, 2, and 3, respectively. The NAT refractive indices in Fig. 6 agree well, except at wavenumbers below 1300 cm^{-1}.

The importance of the temperature dependence of the sulfuric acid indices is illustrated in Fig. 7. Room temperature [47] and cold temperature [49] real indices at 900 cm^{-1} differ by 25% and the

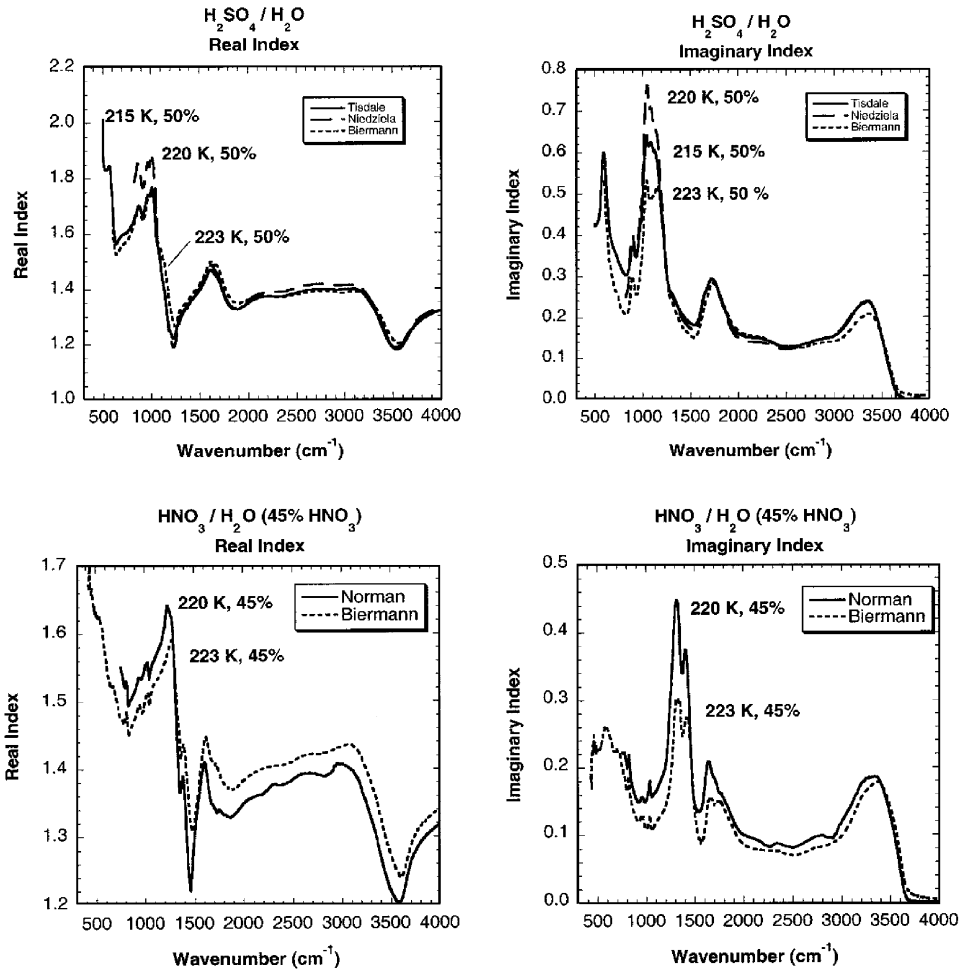

Fig. 8. Intercomparisons of the real and imaginary refractive indices of H_2SO_4/H_2O [46–48] and HNO_3/H_2O at cold stratospheric temperatures [48,50]. The differences point to the need for additional laboratory measurements.

imaginary indices at 1200 cm^{-1} differ by 70%. Sulfuric acid particles in the atmosphere typically have radii below 0.5 μm, thus the size parameter is small enough such that the aerosol spectrum mirrors the wavelength dependence of the imaginary index. Thus, the temperature sensitivity of the imaginary indices displayed in Fig. 7 is important.

There are, however, appreciable differences in the available cold temperature indices of H_2SO_4/H_2O and HNO_3/H_2O (see Fig. 8). Imaginary indices [49–51] at 50% H_2SO_4 for temperatures near 220 K differ by 50% near 1000 cm^{-1}. The data agree fairly well at wavenumbers greater than 1200 cm^{-1}. Comparisons of HNO_3/H_2O indices for 45% HNO_3 are displayed in the bottom panels of Fig. 8. Imaginary indices differ by 50% near 1400 cm^{-1}. Calculations of sulfuric acid and ternary droplet aerosol extinction spectra therefore are problematic due to appreciable uncertainties in both the H_2SO_4/H_2O and HNO_3/H_2O indices.

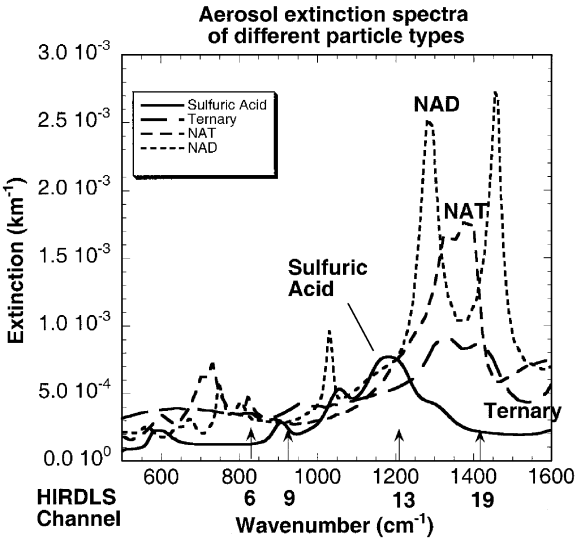

Fig. 9. Theoretical aerosol extinction spectra for sulfuric acid, ternary, NAT and NAD particles. The four HIRDLS radiometric channels that are sensitive to aerosol detection are indicated by short vertical arrows.

3.4. Applications

Particles influence both heterogeneous chemistry and radiative transfer in the troposphere and stratosphere. Particles also impact retrievals of gaseous species for several types of remote sensing instruments. Identification of particle type (and attributes such as the path-averaged particle size distribution and surface area density) is therefore an important task, both from the viewpoint of retrievals and that of data applications.

To illustrate the wavelength dependence of aerosol extinction spectra, we present in Fig. 9 theoretical spectra for stratospheric sulfuric acid aerosol and three PSC particle types (ternary, NAT, and NAD). Eq. (8) was applied using available indices (i.e. Ref. [46] for sulfuric acid droplets, Ref. [51] for NAT and NAD particles, Ref. [50] for ternary particles) and in-situ particle size distributions for sulfuric acid aerosol and PSC particles. It is apparent in Fig. 9 that each particle type has a unique infrared spectral signature. Similar calculations have been used in studies [54,55] to identify aerosol composition types in remote sensing observations.

Four of the 23 HIgh Resolution Dynamics Limb Sounder (HIRDLS, see http://hirdls.eos.ucar.edu/hirdls) radiometer channels are sensitive to aerosol opacity, and are indicated by short vertical lines in Fig. 9. HIRDLS data will be used to measure multi-wavelength aerosol extinction coefficients to identify particle types, and to provide a way to interpolate for the aerosol extinction values at the other radiometer channels.

4. Future developments

The HITRAN tabulation of the cross-sections of atmospheric molecules will grow as satellite experiments develop the capability to observe the stratosphere and troposphere at higher spectral

resolution over a wide range of wavelength. For example, the Tropospheric Emission Spectrometer (TES, see http:/www.jpl.nasa.gov/missions/future/tes.html), and the Michelson Interferometer for Passive Atmospheric Sounding (MIPAS, see http://www-atm.physics.ox.ac.uk/group/mipas), experiments will possibly detect emission features from several species not currently on the HITRAN listing, e.g. benzene, ethylene, propane, acetone, methyl alcohol, peroxyacetlynitrate (PAN), acetic acid, and methyl hydroperoxide. Additional cross-sections that have been measured in the laboratory (e.g. the May et al. [56,57] cross-sections of HNO_4) also need to be added to the future HITRAN database.

As noted above, there is a need for improvements in the determination of the indices of refraction of ternary droplets at relevant stratospheric temperatures. The differences displayed in Figs. 7 and 8 introduce large uncertainties in the calculation of ternary PSC extinction spectra.

Since the present tabulation of indices is for a discrete number of conditions (i.e. temperature, weight percent composition), it is preferable that a semi-empirical specification of the ternary ($H_2SO_4/HNO_3/H_2O$) indices be developed that covers the full range of atmospheric conditions. The accuracy of the semi-empirical specification will of course be dependent upon the accuracy of the discrete data sets.

Acknowledgements

This work was supported by the Earth Observing System (EOS) program of NASA. The National Center for Atmospheric Research is supported by the National Science Foundation.

References

[1] Rothman LS, Barbe A, Benner DC, Brown LR, Camy-Peyret C, Carleer MR, Chance KV, Clerbaux C, Dana V, Devi VM, Fayt A, Nemtchinov V, Flaud J-M, Gamache RR, Goldman A, Jacquemart D, Jucks KW, Lafferty WJ, Mandin J-Y, Massie ST, Newnham DA, Perrin A, Rinsland CP, Schroeder J, Smith KM, Smith MAH, Tang K, Toth RA, Vander Auwera J, Varanasi P, Yoshino K. The HITRAN molecular spectroscopic database: edition of 2000 including updates through 2001. JQSRT 2003, doi:10.1016/S0022-4073(03)00146-8.

[2] Rothman LS, Rinsland CP, Goldman A, Massie ST, Edwards, DP, Flaud J-M, Perrin A, Camy-Peret C, Dana V, Mandin J-Y, Schroeder J, McCann A, Gamache RR, Watson RB, Yoshino K, Chance KV, Jucks KW, Brown LR, Nemtchinov V, Varanasi P. The HITRAN molecular spectroscopic database and HAWKS (HITRAN atmospheric workstation): 1996 edition. JQSRT 1998;60:665–710.

[3] Houghton JT, Callander BA, Varney SK, editors. Climate change 1990: the intergovernmental panel on climate change scientific assessment. New York: Cambridge University Press, 1990.

[4] Clerbaux C, Colin R, Simon PC, Granier C. Infrared cross sections and global warming potentials of 10 alternative hydrohalocarbons. J Geophys Res 1993;98:10491–7.

[5] Varanasi P, Nemtchinov V. Thermal infrared absorption coefficients of CFC-12 at atmospheric conditions. JQSRT 1994;51:679–87.

[6] Montzka SA, Butler JH, Myers RC, Thompson TM, Swanson TH, Clarke AD, Lock LT, Elkins JW. Decline in the tropospheric abundance of Halogen from Halocarbons: implications for stratospheric ozone depletion. Science 1996;272:1318–22.

[7] Montzka SA, Butler JH, Elkins JW, Thompson TM, Clarke AD, Lock LT. Present and future trends in the atmospheric burden of ozone-depleting halogens. Nature 1999;398:690–4.

[8] Orlando JJ, Schauffler S. Halogen compounds. In: Brasseur GP, Orlando JJ, Tyndall GS, editors. Atmospheric chemistry and global change. New York: Oxford University Press, 1999. p. 291–323.

[9] Varanasi P, Nemtchinov V, Li S, Cherukuri A. spectral absorption-coefficient data on HCFC-22 and SF6 for remote sensing applications. JQSRT 1994;52:323–32.
[10] Ballard J, Johnston WB, Gunson MR, Wassell PT. Absolute absorption coefficients of $ClONO_2$ infrared bands at stratospheric temperatures. J Geophys Res 1988;93:1659–65.
[11] Wagner G, Birk M. New infrared spectroscopic database for chlorine nitrate. JQSRT 2003, doi:10.1016/S0022-4073(03)00169-9.
[12] Nemtchinov V, Varanasi P. Thermal infrared absorption cross-sections of CCl_4 needed for atmospheric remote sensing, JQSRT 2003, doi:10.1016/S0022-4073(03)00171-7.
[13] Cantrell CA, Davidson JA, McDaniel AH, Shetter RE, Calvert JG. Infrared absorption cross sections for N_2O_5. Chem Phys Lett 1988;148:358–63. Erratum, Chem Phys Lett 1988;152:274.
[14] Birk M, Wagner G, private communication.
[15] Zou Q, Sun C, Nemtchinov V, Varanasi P. Thermal infrared cross-sections of C_2F_6 at atmospheric temperatures. JQSRT 2003, doi:10.1016/S0022-4073(02)00353-9.
[16] Massie ST, Goldman A, Murcray DG, Gille JC. Approximate absorption cross sections of F12, F11, $ClONO_2, N_2O_5, HNO_3, CCl_4, CF_4$, F21, F113, F114, and HNO_4. Appl Opt 1985;24:3426–7.
[17] Varanasi P. Absorption coefficients of CFC-11 and CFC-12 needed for atmospheric remote sensing and global warming studies. JQSRT 1992;48:205–19.
[18] McDaniel AH, Cantrell CA, Davidson JA, Shetter RE, Calvert JG. The temperature dependent, infrared absorption cross sections for the chlorofluorocarbons: CFC-11, CFC-12, CFC-13, CFC-14, CFC-22, CFC-113, CFC-114, and CFC-115. J Atmos Chem 1991;12:211–27.
[19] Massie ST, Goldman A, McDaniel AH, Cantrell CA, Davidson JA, Shetter RE, Calvert JG. Temperature dependent infrared cross sections for CFC-11, CFC-12, CFC-13, CFC-14, CFC-22, CFC-113, CFC-114, and CFC-115. NCAR Tech Note/TN-358+STR 1991.
[20] Nemtchinov V, Varanasi P. Thermal infrared absorption cross-sections of CF_4 for atmospheric applications. JQSRT 2003, doi:10.1016/S0022-4073(03)00170-5.
[21] Smith K, Newnham D, Page M, Ballard J, Duxbury G. Infrared band strengths and absorption cross-sections of HFC-32 vapour. JQSRT 1996;56:73–82.
[22] Smith K, Newnham D, Page M, Ballard J, Duxbury G. Infrared absorption cross-sections and integrated absorption intensities of HCFC-134 and HFC-143a vapour. JQSRT 1998;59:437–51.
[23] Nemtchinov V, Varanasi P. Absorption cross-sections of HFC-134a in the spectral region between 7 and 12 μm. JQSRT 2003, doi:10.1016/S0022-4073(02)00356-4.
[24] World Meteorological Organization Report No. 44, Scientific assessment of ozone depletion: 1988.
[25] Houghton JT, Ding Y, Griggs DJ, Noguer M, van der Linden PJ, Dai X, Maskell K, Johnson, editors. Climate change 2001: the scientific basis. New York: Cambridge University Press, 2001.
[26] Massie ST. Indices of refraction for the HITRAN compilation. JQSRT 1994;52:501–13.
[27] Carslaw KS, Luo B, Peter T. An analytic expression for the composition of aqueous HNO_3-H_2SO_4 stratospheric aerosols including gas phase removal of HNO_3. Geophys Res Lett 1995;22:1877–80.
[28] Van de Hulst HC. Light scattering by small particles. New York: Wiley, 1957.
[29] Bohren CF, Huffman DR. Absorption and scattering of light by small particles. New York: Wiley, 1983.
[30] Mischencho MI, Hovenier JW, Travis LD, editors. Light scattering by nonspherical particles. San Diego: Academic Press, 2000.
[31] Barber PW, Hill SC. Light scattering by particles. Computational methods. Singapore: World Scientific, 1990.
[32] Yang P, Liou KN. Finite-difference time domain method for light scattered by small ice crystals in three-dimensional space. J Opt Soc Am 1996;13:2072–85.
[33] Liou K-N. An introduction to atmospheric radiation. New York: Academic, 1980.
[34] Thomas GE, Stamnes K. Radiative transfer in the atmosphere and ocean. New York: Cambridge University Press, 1999.
[35] Downing HD, Williams D. Optical constants of water in the infrared. J Geophys Res 1975;80:1656–61.
[36] Kou L, Labrie D, Chylek P. Refractive indices of water and ice in the 0.65 to 2.5 micron range. Appl Opt 1993;32:3531–40.
[37] Warren SG. Optical constants of ice from the ultraviolet to the microwave. Appl Opt 1984;23:1206–25.

[38] Clapp ML, Miller RE, Worsnop DR. Frequency-dependent optical constants of water ice observed directly from aerosol extinction spectra. J Phys Chem 1995;99:6317–26.
[39] Rajaram B, Glandorf DL, Curtis DB, Tolbert MA, Toon OB, Ockman N. Temperature-dependent optical constants of water ice in the near infrared: new results and critical review of the available measurements. Appl Opt 2001;40: 4449–62.
[40] Shettle EP, Fenn RW. Models for the aerosols of the lower atmosphere and effects of humidity variations on their optical properties. AFGL-TR-79-0214, 20 September 1979.
[41] Fenn RW, Clough SA, Gallery WO, Good RE, Kneizys FX, Mill JD, Rothman LS, Shettle EP. Optical and infrared properties of the atmosphere. In: Jursa AS, editor. Handbook of geophysics and the space environment. Hanscom AFB, MA: Air Force Geophysics Laboratory, 1985 [chapter 18].
[42] Longtin DR, Shettle EP, Hummel JR, Pryce JD. A wind dependent desert aerosol model: radiative properties. AFGL-TR-88-0112, Air Force Geophysics Laboratory, Hanscom AFB, MA, April 1988.
[43] Hummel JR, Shettle EP, Longtin DR. A new background stratospheric aerosol model for use in atmospheric radiation models, AFGL-TR-88-0166, Air Force Geophysics Laboratory, Hanscom AFB, MA, August 1988.
[44] Palmer KF, Williams D. Optical constants of sulfuric acid; application to the clouds of Venus? Appl Opt 1975;14: 208–19.
[45] Remsberg EE, Lavery D, Crawford B. Optical constants for sulfuric and nitric acids. J Chem Eng Data 1974;19: 263–5.
[46] Tisdale RT, Glandorf DL, Tolbert MA, Toon OB. Infrared optical constants of low-temperature H_2SO_4 solutions representative of stratospheric sulfate aerosols. J Geophys Res 1998;103:25353–70.
[47] Niedziela RF, Norman ML, Deforest CL, Miller RE, Worsnop DR. A temperature and composition-dependent study of H_2SO_4 aerosol optical constants using Fourier transform and tunable diode laser infrared spectroscopy. J Phys Chem A 1999;103:8030–40.
[48] Biermann UM, Luo BP, Peter T. Absorption spectra and optical constants of binary and ternary solutions of H_2SO_4, HNO_3, and H_2O in the mid infrared at atmospheric temperatures. J Phys Chem A 2000;104:783–93.
[49] Querry MR, Tyler IL. Reflectance and complex refractive indices in the infrared of aqueous solutions of nitric acid. J Chem Phys 1980;72:2495–9.
[50] Norman ML, Qian J, Miller RE, Worsnop DR. Infrared complex refractive indices of supercooled liquid HNO_3/H_2O aerosols. J Geophys Res 1999;104:30571–84.
[51] Toon OB, Tolbert MA, Koehler BG, Middlebrook AM, Jordan J. Infrared optical constants of H_2O ice, amorphous nitric acid solutions, and nitric acid hydrates. J Geophys Res 1994;99:25631–54.
[52] Richwine LJ, Clapp ML, Miller RE, Worsnop DR. Complex refractive indices in the infrared of nitric acid trihydrate aerosols. Geophys Res Lett 1995;22:2625–8.
[53] Sutherland RA, Khanna RK. Optical properties of organic-based aerosols produced by burning vegetation. Aerosol Sci Technol 1991;14:331–42.
[54] Rinsland C, Yue GK, Gunson MR, Zander R, Abrams MC. Mid-infrared extinction by sulfate aerosols from the Mt. Pinatubo eruption. JQSRT 1994;52:241–52.
[55] Toon OB, Tolbert MA. Spectroscopic evidence against nitric acid trihydrate in polar stratospheric clouds. Nature 1995;375:218–21.
[56] May RD, Molina LT, Webster CR. Tunable diode laser measurements of HO_2NO_2 absorption coefficients near 12.5 μm. J Phys Chem 1988;92:4667–9.
[57] May RD, Friedl RR. Integrated band intensities of NO_2NO_2 at 220 K. JQSRT 1993;50:257–66.